Nuclear Inst. and Methods in Physics Research, A 976 (2020) 164282

Contents lists available at ScienceDirect

Nuclear Inst. and Methods in Physics Research, A

journal homepage: www.elsevier.com/locate/nima

Optimization of the double micro-mesh gaseous structure (DMM) for low ion-backflow applications

Binbin Qi, Kunyu Liang, Zhiyong Zhang *, Jianxin Feng, Jianbei Liu, Ming Shao, Yi Zhou

State Key Laboratory of Particle Detection and Electronics, University of Science and Technology of China, Hefei 230026, China
Department of Modern Physics, University of Science and Technology of China, Hefei 230026, China

ARTICLE INFO

Keywords:
Ion-backflow
Double-mesh
Micromegas
Space charge effect

ABSTRACT

Micro-pattern gaseous detectors with very low ion-backflow (IBF) provide cost-effective solutions to large-area and position-sensitive photon detection and readouts of high-rate time projection chambers. We have developed a double micro-mesh gaseous structure (DMM) with two avalanche stages, which has a low IBF ratio and high gain. The results of our previous work show that an IBF ratio as low as 0.05% was obtained and a gain of up to 3×10^6 was maintained for single electrons for the DMM. In this study, the DMM was optimized to further suppress its IBF by changing the size of gas gaps and the density of the wire mesh, and more significantly, by aligning the two mesh layers with a crossing angle. An IBF ratio lower than 0.025% was achieved after the structure optimization. There is also an indication that the IBF in the DMM may potentially be further suppressed.

1. Introduction

Low ion-backflow (IBF) detectors have broad application prospects, including gaseous photo detectors (GPD) and time projection chambers (TPC) [1–3]. The GPDs primarily include photon detectors for ring-imaging Cherenkov counters (RICH) [4,5] and gas photomultiplier tubes (gas-PMTs) [6–8]. The effect of ion-backflow may cause aging of the photocathodes of GPDs. The quantum efficiency of a GPD will degrade when its photocathode is bombarded by ions [9,10], which are produced during the gas multiplication process. Thus, the suppression of ion-backflow is necessary to satisfy the demand for high sensitivity and long lifetime of GPDs. For TPCs, the back flowing ions will cause distortion of the electric field in the drift volume, thus degrading the performance of TPCs. Therefore, the study of low IBF detectors is important. Some detector structures, based on micro-pattern gaseous detectors (MPGD), have been studied [11] to suppress the IBF ratio, such as the multiple gas electron multiplier structures (multi-GEMs) [12], hybrid structure [13], cascaded GEM to micro-mesh gaseous structure (Micromegas) [14], and micro-hole and strip plates (MHSP) [8,15].

For the purpose of low IBF applications, a double micro-mesh gaseous structure (DMM) [16,17] with two avalanche stages, was developed using a thermal bonding technique [18]. As presented in our previous work [16], an IBF ratio as low as 0.05% was obtained and a gain of up to 3×10^6 was maintained for single electrons with the DMM structure. To further suppress the IBF of DMMs, the structure was optimized by changing the size of gas gaps between two mesh layers and wire mesh density, and more significantly by aligning the two mesh layers with a crossing angle. A series of DMM prototypes with different parameter settings were fabricated and tested for the structure optimization.

In this paper, the details of the designs of the various DMM prototypes and the method of IBF measurement are described. The performance of the DMM prototypes tested by a copper X-ray gun is presented.

2. DMM prototypes for structure optimization

2.1. DMM gaseous structure

The DMM shown in Fig. 1 is similar to a typical Micromegas; however, it has two layers of mesh to provide cascading avalanche amplification. It has a 3 mm gas gap for particle primary ionization and electron drift, followed by a ~0.2 mm pre-amplification (PA) gas gap and a ~0.1 mm secondary amplification (SA) gap. The double cascading avalanche gaps ensure a high gain for a single electron and, with proper configuration of the electric field, a low IBF ratio [16].

2.2. Optimized design of DMM for IBF suppression

Previous studies have indicated that some critical factors, such as the alignment [17,19,20] and distance between the two meshes, and wire density of the meshes [21], will change the IBF performance of

* Corresponding author at: State Key Laboratory of Particle and Electronics, University of Science and Technology of China, Hefei 230026, China.
E-mail address: zhzhy@ustc.edu.cn (Z. Zhang).

https://doi.org/10.1016/j.nima.2020.164282
Received 13 January 2020; Received in revised form 4 June 2020; Accepted 16 June 2020
Available online 18 June 2020
0168-9002/

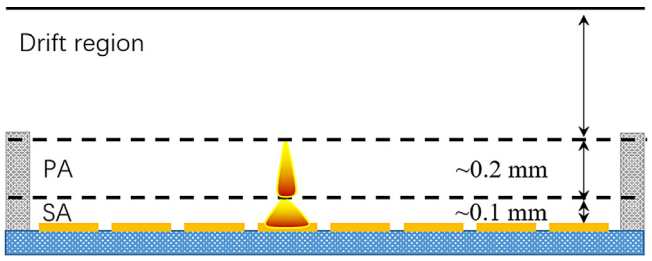

Fig. 1. Schematic design of the DMM.

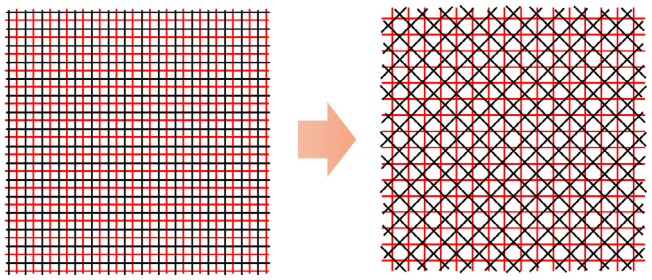

Fig. 2. Schematic diagram of the mesh setting: perfectly misaligned (left) and with a crossing angle (right), the red and the black lines represent different mesh layers, respectively.

the DMM. The meshes used were a type of woven stainless steel, which is industrially mature and easy to obtain.

Firstly, ions are heavier than electrons and tend to move along the direction of the strong electric field in the avalanche gaps. They can therefore be blocked by misaligning the wires of the meshes [17,19,20]. In comparison, electrons could pass through the meshes due to their large transverse diffusion and mean free path. The most effective configuration to make the wires maximally misaligned is shown in Fig. 2 (left). However, it is impractical to make a precise alignment of the meshes because the wire pitch is approximately tens of microns. Therefore, setting a crossing angle is a convenient way to ensure their misalignment. Fig. 2 (right) shows the schematic diagram of the meshes with a crossing angle.

Secondly, the IBF ratio, which varies with the ratio of the ion cloud size (σ) in the avalanche to the mesh pitch (L), was simulated and tested in [21] for a typical Micromegas. The investigation suggested that the IBF ratio can be suppressed by increasing the σ/L value, which can be achieved by enlarging the distance and the wire density of the two meshes. The first DMM prototype, reported in [16], had a mesh type of 500 lines per inch (LPI) and a PA gap of 240 μm. We chose a similar mesh type (650 LPI) for comparison, the detailed parameters of which are shown in Table 1. In addition, a 180 μm distance between the meshes (PA gap) is used as a contrast.

Using the above-mentioned information, several DMMs, with different configurations, were designed and listed in Table 2. Different crossing angles, PA gaps, and wire density of meshes were selected to fabricate the DMM prototypes for the IBF optimization study. Following the design optimization, four DMM prototypes, named DMM1, DMM2, DMM3, and DMM4 (Table 2) were fabricated. DMM1 was the same prototype presented in [16] and the other three were newly fabricated with sensitive area dimensions of 2.5 × 2.5 cm^2 and a SA gap of ~100 μm.

3. Test setup and method

3.1. Test setup

Before the IBF study was performed, an ^{55}Fe source (providing 5.9 keV X-rays) was used to determine DMMs' optimal operation parameters, including the operation voltages for each electrode and the electric

Table 2
DMM prototypes with different parameter settings.

Detectors	Cross angle (°)	PA gaps (μm)	LPI
DMM1	0	240	500
DMM2	45	240	500
DMM3	45	180	500
DMM4	45	240	650

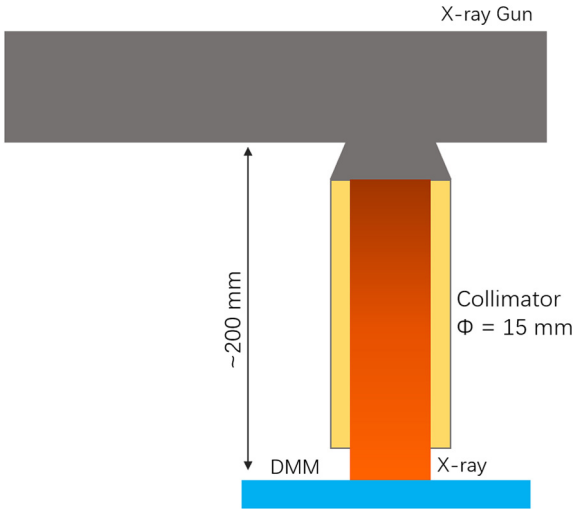

Fig. 3. IBF measurement setting.

field ratio between the pre-amplification and drift volume, and study its primary performance, including energy resolution and gas gain. Then the DMMs were operated at a field ratio (E_{PA}/E_{drift}) of 200 in all tests below to ensure maximum transparency for electrons generated by primary ionization. The gas used was a mixture of 93% Ar and 7% CO_2.

Then a high-intensity X-ray gun was used to study IBF ratio. The IBF ratio was calculated as $(I_{cathode} - I_{primary})/I_{anode}$, where $I_{cathode}$ is the total current measured from the drift cathode, $I_{primary}$ is the current from the primary ions, and I_{anode} is the current from the anode. Because $I_{primary}$ is a very small current, it is usually difficult to measure. Therefore, the high-intensity X-ray gun was used to increase the currents. As shown in Fig. 3, the X-rays were collimated using a copper tube, which had an internal diameter of 15 mm and was 200 mm in length. An X-ray intensity of ~50 kHz/cm^2 (recorded by the DMM) with an irradiation area of ~180 mm^2 enabled the $I_{primary}$ to increase higher than 5 pA, which was significant enough for measurement. The currents were measured using a Keithley picoammeter [22] with a resolution of ~10 fA at a dynamic range of ± 20 nA. The details of the measurement method are the same as that of [16,17].

3.2. Validation of IBF measurement method

The total gas gain of the DMM can be calculated with the ratios of currents or charges between its anode and drift electrode. The full energy peak of the X-ray spectrum was measured using a charge sensitive pre-amplifier, a shaping amplifier, and a multichannel analyzer (MCA). The charge collected from the anode Q_{anode} for an X-ray was then estimated by calibrating the linear correlation between the input charge and output MCA channel of this electronics chain with a pulse generator. The charge of the primary electrons $Q_{primary}$ was approximately 200 e- for a 5.9 keV X-ray in the Ar+CO_2 gas. Thus, G_q and G_i are defined as $Q_{anode}/Q_{primary}$ and $I_{anode}/I_{primary}$. The gas gains of the DMMs in each high-voltage configuration were tested using the following methods: 5.9 keV low rate X-rays were used for G_q and 8.0 keV high rate X-rays were used for G_i measurements. Fig. 4 shows

Table 1
Parameters of two mesh types.

Type (LPI)	Aperture (μm)	Wire diameter (μm)	Pitch (μm)	Opening rate	Thickness (μm)
500	32	19	51	39.4%	27
650	25	14	39	41.1%	23

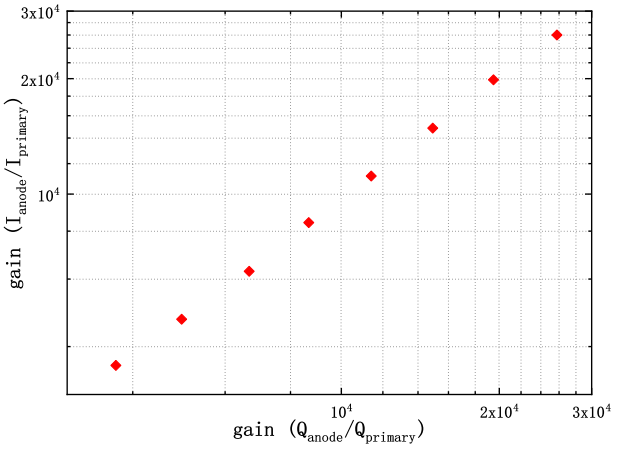

Fig. 4. Consistency between two gains estimated by different methods, $Q_{\text{full-energy-peak}}/Q_{\text{primary}}$ and $I_{\text{anode}}/I_{\text{primary}}$.

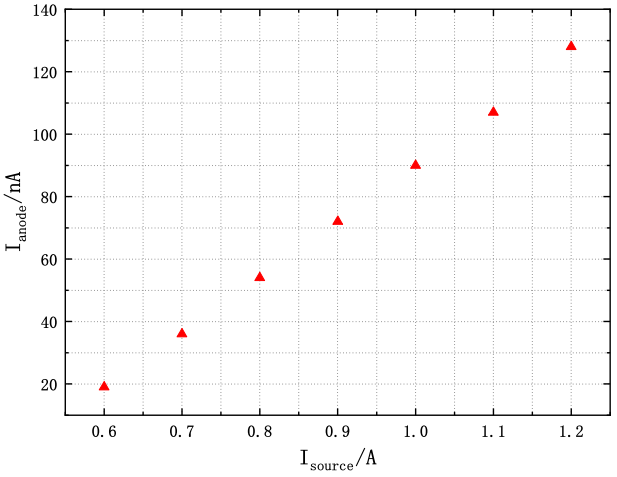

Fig. 5. I_{anode} varies with I_{source}, where I_{source} is the working current of the X-ray gun, which is proportional to the X-ray intensity.

the correlation of G_q and G_i; good consistency between them was observed. However, the counting rate of the X-rays may affect the gas gain and raise uncertainties for the two gains, which were obtained in different X-ray counting rates. The gain stability of the DMM was also studied with different X-ray rates by tuning the working current I_{source} to electron emission of the X-ray gun. The linearity between the anode current of the DMM and I_{source} (shown in Fig. 5) indicates the gain stability under the different X-ray counting rates, which were investigated.

3.3. Space charge effect

Another uncertainty in the IBF measurement is from the space charge effect caused by the feedback ions in the drift volume. Because the drift velocity of ions is very low, the feedback ions will eventually accumulate in the drift volume, resisting the new incoming ions and biasing the I_{drift} measurement, especially in the high X-ray density case [2]. This effect was tested by fixing the high voltages of the DMM

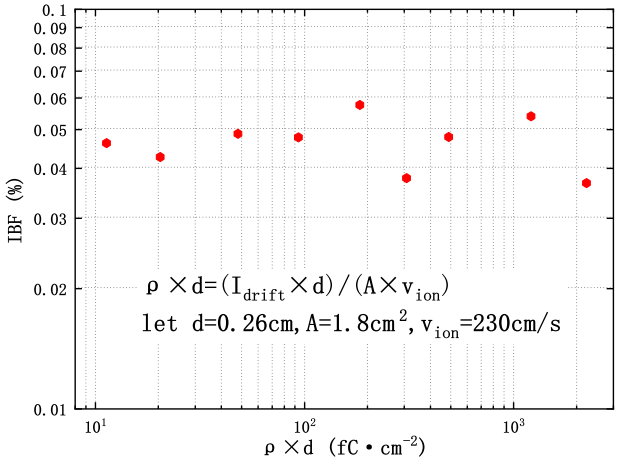

Fig. 6. IBF as a function of space charge density, with all potentials. The increase in space charge density was due to the increase of the X-ray rate.

and varying the irradiation intensity of the X-rays. The space charge density in the drift volume ρ was estimated as $I_{\text{drift}}/(A \cdot v_{\text{ion}})$, where A is the irradiation area of the X-rays and v_{ion} is the drift velocity of ions for a given electric drift field in a gas mixture. In the argon-based gas mixture, the ion drift velocity was approximately 230 cm/s at 150 V/cm. The size of the irradiation spot at the DMM was approximately 1.8 cm^2.

In Fig. 6, the IBF ratio is plotted as a function of $\rho \times d$, where d is the thickness of the drift volume. As demonstrated in [2], the IBF ratio measurement has a sharp break down when $\rho \times d$ exceeds a few 10^4 fC/cm^2. Owing to the very low IBF ratio in the DMM, even when a high X-ray counting rate of up to 30 MHz/cm^2 is selected, the charge density in the drift volume can only reach a value lower than 3000 fC/cm^2, which is much lower than the breakdown threshold of 5×10^4 [2]. All IBF measurements presented in this paper were executed at a $\rho \times d$ value < 100 fC/cm^2, and would thus be resistant to the ion space charge effect.

4. Results and discussion

4.1. Gas gain and energy resolution

The dependence of gas gains and energy resolutions of the DMMs on high voltages were investigated to determine the working points by using 5.9 keV X-rays from an ^{55}Fe source. The DMMs were operated with single amplification stage as a typical MicroMegas to test the PA and SA gas gains individually, and with the combination of two-stage avalanches of PA and SA to test the total gain. Fig. 7 shows the gas gain and energy resolution of the DMM4 prototype, which had the best IBF suppression. A total gain (PA + SA) of 3×10^4 was obtained with an energy resolution of 20% (FWHM). Because of the large amount of charge produced in the SA gap which has a high probability of triggering a spark, the maximum total gain is close to the SA gain, and even worse than the maximum PA gain. Besides, the combined resolution (PA+SA) remained almost constant and was close to the PA resolution, suggesting an almost complete collection of primary electrons for the high-voltage configurations that were used.

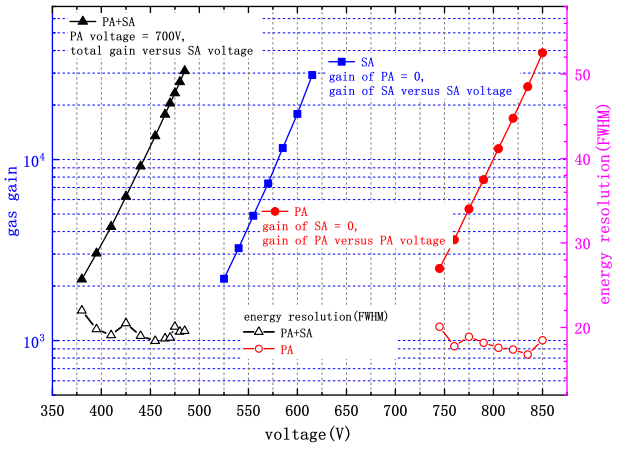

Fig. 7. Gas gain and energy resolution (FWHM) of DMM4 (see Table 2) tested with an ^{55}Fe X-ray source.

4.2. IBF ratios of four DMM prototypes and their comparison

The IBF ratios of the four DMM prototypes were tested by varying the total gain. This was done by fixing the PA voltage and varying the SA voltage. Two DMMs were compared at a time, having only one characteristic different to each other, as detailed in Table 2. Fig. 8 shows the IBF ratios versus total gain for two DMMs with different crossing angles, at fixed PA voltages of 550 V and 650 V. DMM1 and DMM2 had crossing angles of 0° and 45°, respectively. Both were fabricated with 500 LPI meshes and a PA gap of ~240 μm. The results show that a smaller IBF ratio was obtained when the detector had a lower PA voltage, at the same gain. Because of mesh misalignment, the detector with a cross angle had a lower IBF than the one with no angle, at the same total gain. The best IBF ratios obtained by DMM1 and DMM2 were ~0.05% and ~0.04%, respectively, indicating that the application of the cross angle to two meshes was advantageous for suppressing the IBF ratio.

Fig. 9 shows the IBF ratio versus the total gain for two detectors with different PA gaps. The different PA voltages of two detectors are chosen, due to their different PA gap sizes. DMM2 and DMM3 had PA gaps of 240 μm and 180 μm, respectively. Both DMMs had a cross angle of 45° and were made of 500 LPI mesh. The results show that DMM2 had a lower IBF ratio than DMM3, indicating that a larger PA gap is conducive to reducing the IBF ratio. The large PA gap improved the electron diffusion, which prevented the ions produced from pre-amplification from flowing back into the drift volume [21].

Fig. 10 shows the IBF ratio versus the total gain with a fixed PA voltage (550 V and 650 V) for two detectors with different mesh types. DMM2 and DMM4 were made of 500 and 650 LPI meshes, respectively. Both detectors have a cross angle of 45° and a PA gap of 240 μm. An IBF ratio as low as 0.025% was obtained by DMM4, which was much smaller than that of DMM2. When the mesh had a high LPI, the electrons easily diffused to the volume at which the electric field lines terminate at the upper mesh. Thus, the ions produced in this volume did not flow back into the drift volume, causing a low IBF ratio.

All the results mentioned above are presented together in Fig. 11a. The lowest IBF ratio, of 0.025%, was obtained by DMM4 when it operated with a PA voltage of 550 V and a total gain of ~20 000. The results indicate that to decrease the IBF ratio down to an optimal level, a low PA electric field, a large PA gap, a high mesh density, and a crossing mesh are required. Fig. 11b shows the product of the IBF ratio and gain value versus the total gain. Most of the plots decrease lower than 5, for a total gain of 5000, which fulfills the requirement for applications in high-rate TPC [1,13].

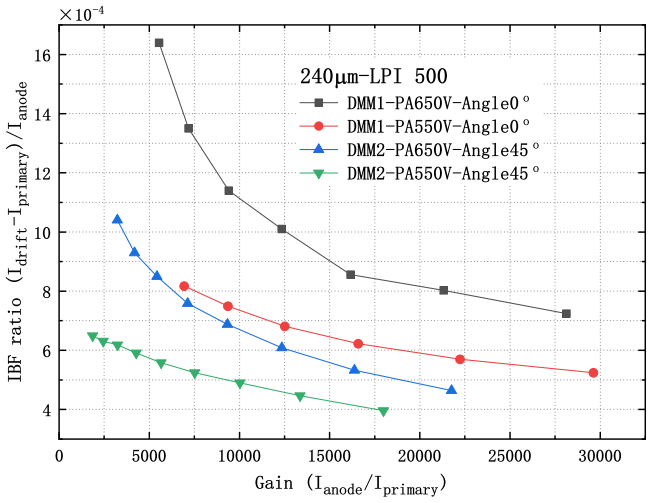

Fig. 8. IBF ratio versus total gain, with fixed PA voltages of 550 V and 650 V, respectively, for two detectors with different cross angles.

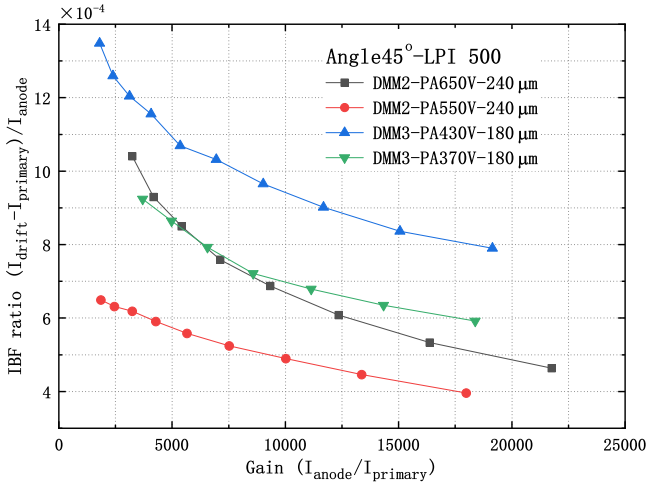

Fig. 9. IBF ratio versus total gain for two detectors with different PA gaps.

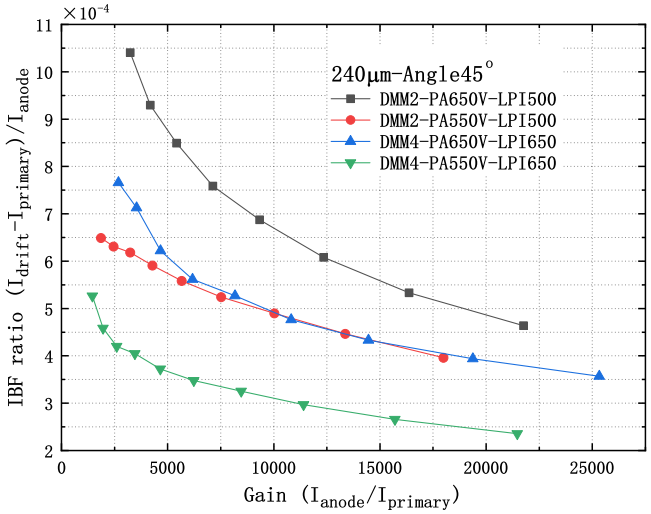

Fig. 10. IBF ratio versus total gain with a fixed PA voltage of 550 V and 650 V, respectively, for two detectors with different mesh types.

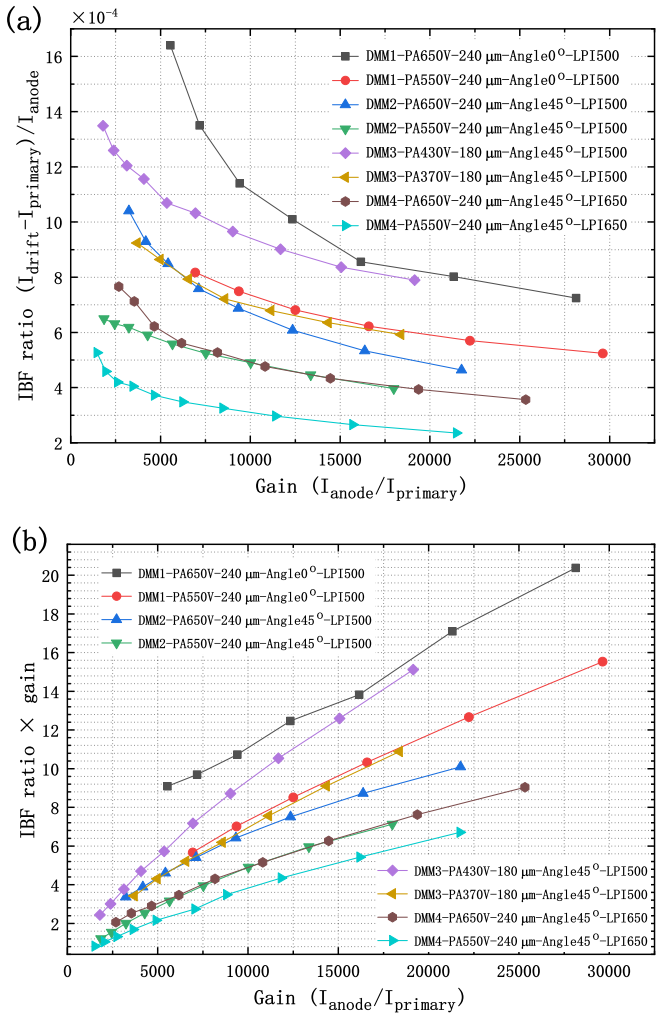

Fig. 11. (a) IBF ratio versus total gain with a fixed PA voltage, for all detectors; (b) the product of the IBF ratio and gain versus the total gain.

4.3. Stability of the DMM

Long-term stability is important for the performance of a gaseous detector. The sparks in the amplification gap cause a dead time and possible long-term damage [23]. Therefore, the spark probability of the DMM must be tested to confirm that it remains at a low level. As shown in Fig. 12, the anode current of the DMM was measured over 20 h, at a gain of 5000, by an 8.0 keV X-ray with a rate of ∼50 kHz. In the figure, each current spike represents one discharge. The fluctuation of the current curve over a long time scale was caused by the instability of the X-ray gun. The spark probability can be estimated by counting the number of spikes and the total number of X-ray signals in the curve. There were only a few spikes in the curve, however, the total number of X-ray signals in 20 h was over 3×10^9. Thus, the spark probability of the DMM was less than 10^{-9}, which indicates good stability.

5. Conclusion

A series of DMM prototypes with differing crossing angles, PA gaps, and mesh types were fabricated and investigated using X-rays (5.9 keV from ^{55}Fe source and 8.0 keV from an X-ray gun). The results of this investigation indicate that a low PA voltage, large PA gap, high mesh density, and crossed mesh setting improves IBF suppression at the same total gain. A low IBF ratio, as low as 0.025%, was obtained at a PA voltage of 550 V for DMM4, which was made of 650 LPI mesh and had a PA gap of 240 μm and a cross angle of 45°. The measurement method for the gas gains and currents was validated. The ion space charge effect was studied and verified to be negligible in the case of very low IBF ratio in a DMM. The stability of the DMM prototype was also measured with a low sparking probability, smaller than 10^{-9} in a test done over 20 h. These features of the DMM present its strong potential for Gas-PMTs, RICH photoelectric readout, and high-rate TPCs.

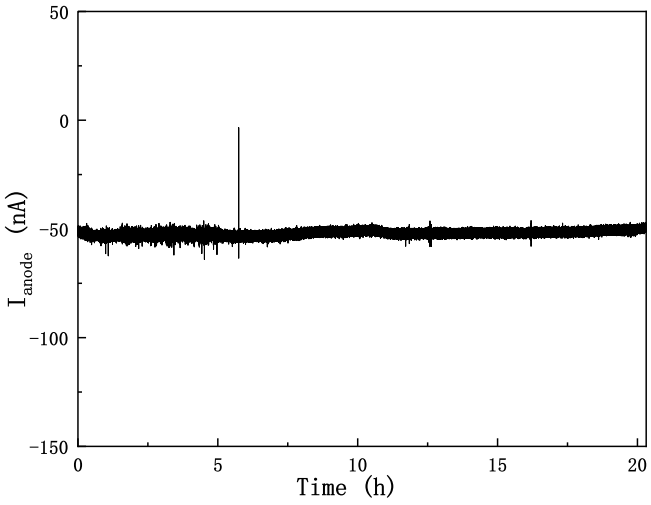

Fig. 12. Anode current of the DMM4 at a gain of 5000, recorded over 20 h. Each current spike represents one discharge.

CRediT authorship contribution statement

Binbin Qi: Validation, Methodology, Investigation, Formal analysis, Data curation, Writing - original draft, Writing - reviewing & editing. **Kunyu Liang:** Validation, Methodology, Formal analysis, Data curation. **Zhiyong Zhang:** Conceptualization, Methodology, Investigation, Writing - reviewing & editing, Supervision, Project administration. **Jianxin Feng:** Writing - reviewing & editing. **Jianbei Liu:** Writing - reviewing & editing, Supervision, Project administration, Resources, Funding acquisition. **Ming Shao:** Writing - review & editing. **Yi Zhou:** Writing - review & editing.

Declaration of competing interest

The authors declare that they have no known competing financial interests or personal relationships that could have appeared to influence the work reported in this paper.

Acknowledgments

This work was supported by the National Key Programme for S&T Research and Development [Grant No. 2016YFA0400400]; the Program of National Natural Science Foundation of China [Grant No. 11935014, 11605197]; the Double First-Class university project foundation of USTC; and the Fundamental Research Funds for the Central Universities. The authors wish to thank Hefei Comprehensive National Science Center for their strong support. This work was partially carried out at the USTC Center for Micro and Nanoscale Research and Fabrication, we thank Dianfa Zhou for his help on the laser cutting of thermal bonding films.

References

[1] D.S. Bhattacharya, P. Bhattacharya, P.K. Rout, et al., Experimental and numerical simulation of a TPC like set up for the measurement of ion backflow, Nucl. Instrum. Methods Phys. Res. A 861 (2017) 64–70.

[2] M. Ball, K. Eckstein, T. Gunji, Ion backflow studies for the ALICE TPC upgrade with GEMs, J. Instrum. 9 (2014) C04025.

[3] F. Sauli, L. Ropelewski, P. Everaerts, Ion feedback suppression in time projection chambers, Nucl. Instrum. Methods Phys. Res. A 560 (2006) 269–277.

[4] M. Alexeev, R. Birsa, F. Bradamante, et al., THGEM-Based photon detectors for the upgrade of COMPASS RICH-1, Nucl. Instrum. Methods Phys. Res. A 732 (2013) 264–268.

[5] M. Alexeev, R. Birsa, F. Bradamante, et al., The quest for a third generation of gaseous photon detectors for cherenkov imaging counters, Nucl. Instrum. Methods Phys. Res. A 610 (2009) 174–177.

[6] K. Matsumoto, T. Sumiyoshi, F. Tokanai, et al., Ion-feedback suppression for gaseous photomultipliers with micro pattern gas detectors, Physics Procedia 37 (2012) 499–505.

[7] F. Tokanai, T. Moriya, M. Takeyama, et al., Newly developed gaseous photomultiplier, Nucl. Instrum. Methods Phys. Res. A 766 (2014) 176–179.

[8] A.V. Lyashenko, A. Breskin, R. Chechik, et al., Development of high-gain gaseous photomultipliers for the visible spectral range, J. Instrum. 4 (2009) P07005.

[9] J. Va'vra, A. Breskin, A. Buzulutskov, et al., Study of CsI photocathodes: volume resistivity and ageing, Nucl. Instrum. Methods Phys. Res. A 387 (1997) 154–162.

[10] T. Moriya, F. Tokanai, K. Okazaki, et al., A concise quantum efficiency measurement system for gaseous photomultipliers, Nucl. Instrum. Methods Phys. Res. A 732 (2013) 269–272.

[11] S. Dalla Torre, Status and perspectives of gaseous photon detectors, Nucl. Instrum. Methods Phys. Res. A 639 (2011) 111–116.

[12] A. Bondar, A. Buzulutskov, L. Shekhtman, et al., Study of ion feedback in multi-GEM structures, Nucl. Instrum. Methods Phys. Res. A 496 (2003) 325–332.

[13] Y.L. Zhang, H.R. Qi, B.T. Hu, et al., A hybrid structure gaseous detector for ion backflow suppression, Chin. Phys. C 41 (2017) 056003.

[14] Y. Giomataris, Ph. Rebourgeard, J.P. Robert, et al., MICROMEGAS: a high-granularity position-sensitive gaseous detector for high particle-flux environments, Nucl. Instrum. Methods Phys. Res. A 376 (1996) 29–35.

[15] A. Lyashenko, A. Breskin, R. Chechik, et al., Efficient ion blocking in gaseous detectors and its application to gas-avalanche photomultipliers sensitive in the visible-light range, Nucl. Instrum. Methods Phys. Res. A 598 (2009) 116–120.

[16] Z. Zhang, B. Qi, C. Liu, et al., A high-gain, low ion-backflow double micro-mesh gaseous structure for single electron detection, Nucl. Instrum. Methods Phys. Res. A 889 (2018) 78–82.

[17] Z. Zhang, B. Qi, M. Shao, et al., Study on the double micro-mesh gaseous structure (DMM) as a photon detector, Nucl. Instrum. Methods Phys. Res. A 952 (2020) 161978.

[18] J. Feng, Z. Zhang, B. Qi, et al., Thermal bonding method for fabricating micromegas detector and its applications, 2019, arXiv:1910.03170, available at https://arxiv.xilesou.top/abs/1910.03170.

[19] P. Bhattacharya, D.S. Bhattacharya, S. Mukhopadhyay, et al., Investigation of ion backflow in bulk micromegas detectors, J. Instrum. 10 (2015) P09017.

[20] F. Jeanneau, M. Kebbiri, V. Lepeltier, Ion back-flow gating in a micromegas device, Nucl. Instrum. Methods Phys. Res. A 623 (2010) 94–96.

[21] P. Colas, I. Giomataris, V. Lepeltier, Ion backflow in the micromegas TPC for the future linear collider, Nucl. Instrum. Methods Phys. Res. A 535 (2004) 226–230.

[22] Keithley-low-level-sensitive-and-specialty-instruments, available at Keithley-series-6400-picoammeters-manual-0/6482-901-01.pdf. https://www.tek.com.cn.

[23] S. Aune, J. Ball, G. Charles, et al., Origin and simulation of sparks in MPGD, J. Instrum. 7 (2012) C06009.